Fast and Broadband Fiber Dispersion Measurement with Dense Wavelength Sampling

Giorgio M. Ponzo, Marco N. Petrovich*, Xian Feng, Peter Horak, Francesco Poletti, Periklis Petropoulos and David J. Richardson

Optoelectronics Research Centre, University of Southampton, Southampton, SO17 1BJ, UK
*mnp@orc.soton.ac.uk

Abstract: We report on a method to obtain accurate dispersion measurements from spectral-domain low-coherence interferograms, which enables high accuracy (~ps/nm/km), broadband measurements and the determination of very dense (up to 20 points/nm over 500 nm) datasets for both dispersion and dispersion slope. The method exploits a novel phase extraction algorithm which allows the phase associated with each sampling point of the interferogram to be calculated and provides for very accurate results as well as a fast measurement capability, enabling close to real time measurements. The important issue of mitigating the measurement errors due to any residual dispersion of optical elements and to environmental fluctuations was also addressed. We performed systematic measurements on standard fibers which illustrate the accuracy and precision of the technique, and we demonstrated its general applicability to challenging problems by measuring a carefully selected set of fibres: a lead silicate microstructured fiber with a flat, near-zero dispersion profile; a hollow core photonic bandgap fiber with strongly wavelength-dependent dispersion and dispersion slope; a small core, highly birefringent index guiding microstructured fiber, for which polarization resolved measurements over an exceptionally wide (~1000 nm) wavelength interval were obtained.

OCIS codes: (060.2300) Fiber measurements; (060.2270) Fiber characterization ; (060.5295) Photonic crystal fibers; (060.4005) Microstructured fibers.

References and links

1. A. M. Heidt, "Pulse preserving flat-top supercontinuum generation in all-normal dispersion photonic crystal fibers," J. Opt. Soc. Am. B 27, 550-559 (2010).
2. A. Camerlingo, X. Feng, F. Poletti, G.M. Ponzo, F. Parmigiani, P. Horak, M.N. Petrovich, P. Petropoulos, W.H. Loh, and D.J. Richardson, "Near-zero dispersion, highly nonlinear lead-silicate W-type fiber for applications at 1.55 μm," Opt. Express 18, 15747-15756 (2010).
3. J. P. Gordon, "Theory of the Soliton Self-Frequency Shift," Opt Lett 11, 662-664 (1986).
4. V.I. Kruglov, C. Aguergaray, and J.D. Harvey, "Propagation and breakup of pulses in fiber amplifiers and dispersion-decreasing fibers with third-order dispersion," Phys. Rev. A 84, 023823 (2011).
5. M. Taki, A. Mussot, A. Kudlinski, E. Louvergneaux, M. Kolobov, and M. Douay, "Third-order dispersion for generating optical rogue solitons," Phys. Lett. A 374, 691-695 (2010).
6. X. Feng, F. Poletti, A. Camerlingo, F. Parmigiani, P. Petropoulos, P. Horak, G.M. Ponzo, M.N. Petrovich, J. Shi, W.H. Loh, and D.J. Richardson, "Dispersion controlled highly nonlinear fibers for all-optical processing at telecoms wavelengths," Opt. Fiber Technol. 16, 378-391 (2010).
7. C. Lin, A.F. Tynes, A. Tomita, P.L. Liu, D.L. Philen, "Chromatic Dispersion Measurements in Single-Mode Fibers Using Picosecond InGaAsP Injection Lasers in the 1.2-to 1.5-μm Spectral Region", Bell System Technical Journal (1983).
8. B. Costa, M. Puleo, E. Vezzoni, "Phase-shift technique for the measurement of chromatic dispersion in single-mode optical fibres using LEDs", Electron. Lett, 19(25), 1074-1076 (1983).

9. P.L. Francois, F. Alard, and M. Monerie, "Chromatic Dispersion Measurement from Fourier-Transform of White-Light Interference Patterns," Electron Lett 23, 357-358 (1987).
10. M.J. Gander, R. McBride, J.D.C. Jones, D. Mogilevtsev, T.A. Birks, J.C. Knight, P.S.J. Russell, "Experimental measurement of group velocity dispersion in photonic crystal fibre", Electron. Lett.s, 35(1), 63-64 (1999).
11 J. Jasapara, T. H. Her, R. Bise, R. Windeler, and D. J. DiGiovanni, "Group-velocity dispersion measurements in a photonic bandgap fiber," J. Opt. Soc. Am. B 20, 1611-1615 (2003).
12. J. Stone and L. G. Cohen, "Minimum-Dispersion Spectra of Single-Mode Fibers Measured with Subpicosecond Resolution by White-Light Cross-Correlation," Electron. Lett. 18, 716-718 (1982).
13. P. Merritt, R. P. Tatam, and D. A. Jackson, "Interferometric Chromatic Dispersion Measurements on Short Lengths of Monomode Optical Fiber," J. Lightwave Technol. 7, 703-716 (1989).
14. M. A. Ettabib, L. Jones, J. Kakande, R. Slavik, F. Parmigiani, X. Feng, F. Poletti, G. M. Ponzo, J. D. Shi, M. N. Petrovich, W. H. Loh, P. Petropoulos, and D. J. Richardson, "Phase sensitive amplification in a highly nonlinear lead-silicate fiber," Opt. Express 20, 1629-1634 (2012).
15. A. Camerlingo, F. Parmigiani, X. Feng, F. Poletti, W. H. Loh, D. Richardson, and P. Petropoulos, "160-to-40Gibt/s Time Demultiplexing in a low dispersion Lead-Silicate W-index Profile Fiber," in OFC/NFOEC 2011, Los Angeles 6-10 March 2011 (Optical Society of America, 2011), paper OThS6.
16. G. M. Ponzo, X. Feng, P. Horak, F. Poletti, M. N. Petrovich, W. H. Loh, and D. Richardson, "Flat, Broadband Supercontinuum Generation at Low Pulse Energies in a Dispersion-Tailored Lead-Silicate Fibre," in ECOC 2011, Geneva, Switzerland 18-22 Sept 2011 paperWe.10.P1.09.
17. G. Bouwmans, F. Luan, J. C. Knight, P. S. J. Russell, L. Farr, B. J. Mangan, and H. Sabert, "Properties of a hollow-core photonic bandgap fiber at 850 nm wavelength," Opt Express 11, 1613-1620 (2003).
18. M. N. Petrovich, F. Poletti, A. van Brakel, and D. J. Richardson, "Robustly single mode hollow core photonic bandgap fiber," Opt Express 16, 4337-4346 (2008).

1. Introduction

The accurate measurement of the group velocity dispersion (GVD) of optical fibers over wide wavelength intervals (up to several hundred nanometers) is of great importance for the efficient exploitation of nonlinear optical effects. For instance, the precise knowledge of the wavelength dependent dispersion profiles, including the position of any zero-dispersion points, is essential for optimizing the shape and spectral extent of supercontinuum generation [1], or to ensure phase matching conditions in parametric processes [2], or to control effects such as pulse compression and soliton self-frequency shift [3]. It is often also desirable to obtain dense GVD datasets composed of closely spaced data points as the latter enable to reliably determine the higher dispersion orders, which are critical e.g. for applications involving pulse compression [4] and soliton generation [5]. As the above mentioned applications typically require relatively short device lengths (of a few meters to few tens of meters), the ability to measure short samples is of great value. Microstructured optical fibers (MOFs), incorporating arrays of wavelength-scale air holes (or other high-index-contrast features) afford great flexibility in designing the fiber GVD as well as the other linear and nonlinear transmission properties. However, often the dispersion of MOFs is very sensitive to the fiber's structural parameters and small differences between idealized structures and real fibers mean that state-of-the-art modeling tools often cannot provide fully reliable predictions [6]. Thus, a dispersion measurement technique that can provide high accuracy and dense datasets over broad wavelength intervals is paramount for both fiber development and application work.

Several well established techniques exist to measure dispersion in optical fibers, particularly at telecom wavelengths. Here, time-of-flight [7] and phase shift [8] techniques are commonly employed; however, these require very long fiber lengths of the order of tens of km. On the other hand, dispersion measurement techniques that can use short fiber samples are commonly based on low-coherence interferometry (LCI). In these methods, interferograms are produced by combining two broadband beams, one directed through the fiber under test, and the other (reference beam) directed through a free-space variable delay line. The interference can be detected either in the time domain [9,10], typically by varying

the length of the delay line, or in the spectral domain [11-13], by using a scanning monochromator or optical spectrum analyzer (OSA). In the spectral domain, the wavelength dependent GVD can in principle be extracted from single-shot interferograms, which can extend over intervals as wide as several hundred nm. The information on the fiber dispersion (as well as higher dispersion orders) is contained in the phase of the interferogram. To retrieve the phase from the wavelength dependent intensity, two methods are widely employed. The first consists in finding the intensity maxima (or equivalently of the minima), which correspond to a 2π phase shift [12]. This straightforward approach has however the drawback of significantly under-exploiting the information contained in the interferogram as it only outputs a small set of phase values from which the GVD is determined and thus in general it cannot yield reliable information on the dispersion slope. In contrast, a direct nonlinear fit [13] of the interferogram can in principle yield denser datasets, however this approach requires the initial conditions to be set on a case-by-case basis and extensive verification of the quality of the fit, which is very time consuming and often leads to sub-optimal results.

In this work, we present a novel LCI method based on a direct phase extraction scheme, which achieves a combination of broad bandwidth (several hundred nm), dense wavelength sampling intervals and ~ps/nm/km accuracy from single shot measurements. More importantly, it provides for a fast measurement capability, without need for complex off-line data analysis, and is thus amenable to automation. We report systematic measurements demonstrating the accuracy and precision of the technique and its resilience against environmental drifts and disturbances. To further illustrate the versatility of our method, we apply it to the case of three microstructured optical fiber types with widely ranging dispersion profiles.

2. Direct Phase Extraction Method

To introduce the data analysis method we start by considering a basic schematic of a SD-LCI measurement setup, such as the one based on a Mach-Zehnder interferometer shown in Fig. 1(a). The output of a broadband light source is split into two beams, one propagating in the test fiber and a second propagating in air, here assumed a virtually dispersion-free medium. The two beams are then combined and measured using an OSA. If $I_F(\lambda)$ and $I_R(\lambda)$ are the intensities of the fiber and reference beam, respectively, the wavelength dependent intensity recorded at the combiner is given by the well-known equation:

$$I(\lambda) = I_F(\lambda) + I_R(\lambda) + 2V(\lambda)\sqrt{I_F(\lambda)I_R(\lambda)} \cdot \cos[\phi(\lambda)] \quad (1)$$

The oscillatory part depends on the phase difference between the two paths, $\phi(\lambda)$, and it contains an envelope term, termed as the *visibility* of the interferogram, $V(\lambda) < 1$, which effectively defines the interferogram width. Under general conditions, it can be shown that the visibility is a function of the resolution of the OSA and of the dispersive properties of the fiber itself. The phase contains the information about the dispersion of the test fiber as it is related to the fiber's propagation constant $\beta_F(\lambda)$ via the following equation:

$$\phi(\lambda) = \beta_F(\lambda)L - 2\pi d/\lambda \quad (2)$$

where L and d are the length of the test fiber and of the reference arm, respectively. The phase can also be expressed via a Taylor series expansion at an arbitrary wavelength, λ_0 as:

$$\phi(\lambda) = \phi_0 + \phi_1 \cdot (\lambda - \lambda_0) + \phi_2 \cdot (\lambda - \lambda_0)^2 + \phi_3 \cdot (\lambda - \lambda_0)^3 + \cdots \quad (3)$$

The terms ϕ_i, $i = 1,2,3$ in the expansion are related to the optical path difference, the differential group delay and the group velocity dispersion (at λ_0), respectively; higher order terms (not explicitly shown in Eq. 3) are related to higher dispersion orders.

An example of interferogram obtained from a standard single mode fiber (SMF) is shown in Fig. 1(b). It is characterized by spectral fringes having a wavelength dependent spacing, with the maximum spacing occurring at local centers of symmetry (CoSs), in which the phase is stationary and the group delays of the two interferometer arms are exactly matched. The direct extraction of the phase value associated with each point of the interferogram is obtained by solving Eq. (1) with respect to $\phi(\lambda)$, which requires three separate steps: i) normalization for the spectrum of the source, ii) normalization for the envelope function and iii) inversion of the cosine function. To perform the first step, the intensities of the reference and fiber arms are independently recorded, and the background normalized interferogram (shown in Fig. 1(c)-1, blue trace) is obtained as follows:

$$I_N(\lambda) = \frac{I(\lambda) - I_F(\lambda) - I_R(\lambda)}{2\sqrt{I_F(\lambda) I_R(\lambda)}} = V(\lambda) \cdot \cos[\phi(\lambda)] \quad (4)$$

To extract the fringes, I_N must be divided by the visibility, $V(\lambda)$. As the latter depends on the phase derivative and thus on the dispersion, it is necessary to determine empirically the envelope from the measured interferogram. We do this by identifying the maxima and minima and reconstruct $V(\lambda)$ through a linear interpolation of the maxima and the absolute values of the minima of the various fringes, see Fig. 1(c)-2. Such procedure can be implemented via simple algorithms and has been verified to provide an accurate end result despite the seemingly coarse linear approximation. The normalized interferogram is then divided by the envelope (see Fig 1(d)-3, blue trace). It should be noted that this operation is carried out where the interferogram is at the most visible, and thus $V(\lambda) \neq 0$. Finally, the extraction of the phase requires the calculation of the inverse cosine, i.e.:

$$\phi(\lambda) = arccos\left[\frac{I_N(\lambda)}{V(\lambda)}\right] \quad (5)$$

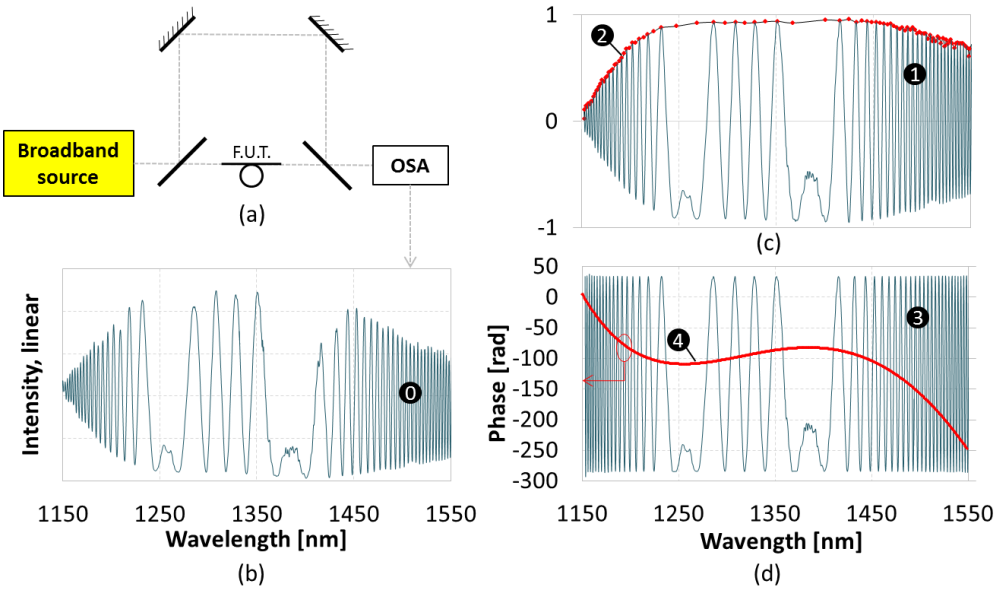

Figure 1: (a) Schematic of a generic spectral domain low-coherence interferometry (SD-LCI) setup based on a Mach-Zehnder topology; (b) As-measured interferogram (0) of a standard SMF using setup described in Section 3; (c) "Background" intensity normalised interferogram (1) and extracted envelope (2). The red dots indicate the maxima and absolute values of the minima; (d) Envelope-corrected interferogram (3) and wavelength dependent phase (4) calculated using Eq. 5. No polynomial smoothing was used in this instance.

The solution of Eq. (5) requires the knowledge of all the maxima (to address the 2π ambiguity of arccos) and of the wavelength of the phase inversion points or CoS. The latter can be calculated by defining a 'fringe spacing function' from the position of the zeros of the normalized interferogram and searching for its local maxima and from knowledge of the envelope function (it can be shown that $V(\lambda) = 1$ at the CoSs). One final step is to address the ambiguity of the phase sign due to cosine being an even function. The phase sign is determined experimentally by looking at the direction of the wavelength shift of each CoS (which depends on the sign of the dispersion) when the reference arm length is varied. This operation can be performed very quickly prior to a measurement. The wavelength dependent phase reconstructed following this method in the case of a standard SMF is shown in Fig. 1(d) (red trace). Note that a very smooth and dense dataset is obtained.

Once $\phi(\lambda)$ has been determined, the dispersion can finally be obtained via the following equation:

$$D(\lambda) = -\frac{1}{2\pi cL}\left[2\lambda\frac{d\phi}{d\lambda} + \lambda^2\frac{d^2\phi}{d\lambda^2}\right] \quad (6)$$

which can be obtained by writing the expression of the $\phi_2$coefficient in Eq. (3).

The method described here has a number of advantages over other similar phase extraction methods. Firstly, it provides very dense datasets and it exploits each of the points of the interferogram, including those in close proximity of the CoSs. Since it can be shown that, for a given resolution of the OSA, the spectral extent of the interferogram is maximized when the interferogram is resolved in proximity of its center of symmetry (as shown in Fig.1(c)), this implies that, in addition to better accuracy, the present method generally achieves a wider measurement range as compared to e.g. the phase maxima/minima method. Furthermore, the method does not involve any nonlinear fit and as such is very fast, as opposed to cosine fit methods and other methods based on polynomial fitting of the phase function, which in general require optimization and quality checks of the results. Dispersion datasets calculated through direct numerical differentiation of $\phi(\lambda)$ (Eq. 6) may in some instances contain an undesirable amount of noise. In order to reduce such noise, a polynomial smoothing of the retrieved phase vs. wavelength curve can be used. Note that this operation does not affect the accuracy of the result because the smoothing is performed on a very large dataset and the noise was experimentally observed to be statistical, nor the overall speed is affected as suitable algorithms to automatically optimize the order of the polynomial can be employed. This operation is not mandatory to determine the GVD but is preferable in order to achieve reliable results for higher dispersion orders obtained by further differentiation of Eq. 6.

3. Interferometric Setup and Method Validation

The setup used for the dispersion measurement, shown in Fig. 2, uses a broadband SC source (Fianium SC450, 450-2300 nm) and a free-space Mach-Zehnder interferometer composed of two beamsplitters (BS1, BS2), two mirrors (M1, M2) and two hollow back-reflectors (HR1, HR2) inserted to allow matching of the length of the reference arm to the measurement arm within the coherence length of the source. A polarizer and half-wave plate (P and λ/2) are used to adjust the polarization state of the interfering beams and offer the option of aligning the measurement beam with a specific polarization axis of the fiber under test. Two motorized shutters (S1, S2) allow the two beams to be recorded individually for intensity normalization purposes and in order to check the source stability over time. The optical elements used in our setup were carefully chosen to provide the widest broadband operation whilst ensuring that they introduced the minimum amount of differential dispersion between the two arms. Any significant residual dispersion present along either of the beam paths could cause systematic errors which would require suitable correction, particularly in the case of fibres with flat, near-zero dispersion and when targeting an accurate measurement of the position of zero dispersion wavelengths. We verified that the phase error due to optical components in our

system was negligible by recording the interferogram obtained by eliminating the half-plate, test fiber and microscope objectives and extending the measurement arm through mirrors, so as to have equal path lengths. A maximum phase error of <10 mrad was recorded in the 600-1750 nm wavelength range. We then measured the phase error introduced by the half-wave plate (Thorlabs AHWP05M-1600) by measuring the difference between the phase of two interferograms of a standard single mode fiber obtained with and without the half-wave plate. We finally estimated the phase error of the two microscope objectives used for input/output coupling to the test fiber. The results obtained were in this case small but not negligible and thus dispersion data measured for the half-wave plate and the objective lenses were used in subsequent measurements to compensate for the systematic error.

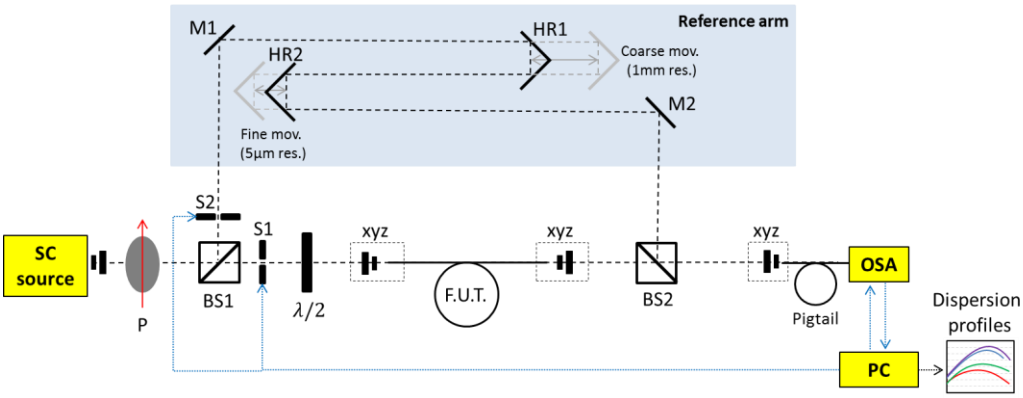

Fig. 2: Setup implemented for the dispersion measurement (refer to text for detailed description). BS1,2: beamsplitter cubes, M1,2: mirrors, HR1,2: hollow back-reflector, P: polarizer; λ/2: half-wave plate; S1,2: motorized beam shutters, xyz: micro-positioner stages used for input/output coupling in the fiber under test.

Another and potentially more serious issue may arise if the relative phase along the two paths is affected by time-varying environmental perturbations (such as drafts, vibrations and temperature drifts). To address such 'temporal stability' issue, complex active stabilization schemes have previously been proposed [12]. We followed a simpler approach and minimized the perturbations by placing our interferometer in an enclosure. To gauge its effectiveness, we measured the dispersion of a standard SMF using OSA scan times ranging from a few seconds to several minutes with such an 'isolated' setup and compared the results with an un-isolated setup. The results are shown in Fig. 3. Whilst for an un-isolated system a relatively short scan time of ~60 s already results in a measurable error of >2 ps/nm/km, for an 'isolated' setup a precision of better than 0.1 ps/nm/km is obtained for scan times as long as 400 s (i.e. well beyond the typical scan times needed to collect a well-resolved interferogram). We thus concluded that simple and cost-effective hermetic enclosures can be very effective in substantially alleviating the temporal stability issue. From these results we concluded that our dispersion measurements can achieve a precision as low as 0.1 ps/nm/km. It should be noted that this estimate includes also possible contributions due to any instabilities in the output intensity of the source, which in principle need to be considered as the measurement and background spectra are collected at different times.

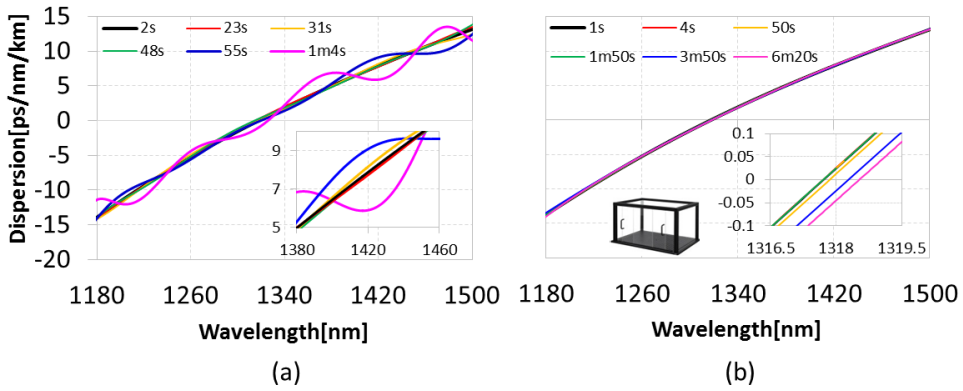

Fig. 3: Evaluation of the measurement precision: the dispersion of a standard single mode fiber is calculated from interferograms obtained by setting increasing OSA scan times and (a) using an un-isolated setup or (b) placing the interferometer inside a hermetic enclosure. The effect of environmental disturbances is very obvious in the first set of plots, while it is almost completely removed in the second.

Further, we investigated the absolute accuracy of our technique by comparing the measured dispersion profiles with the theoretical predictions based on the experimental refractive index profiles of the SMF used in our tests (shown in Fig. 4(a)). Fig. 4(b) shows the excellent agreement between the experimental and simulated data. Our dispersion measurement technique provides an accuracy of better than 0.5 ps/nm/km over at least 400 nm (1200-1600 nm). In order to illustrate the importance of dense wavelength sampling, we also calculated the "theoretical" dispersion slope from the refractive index profile and compared it with experimental data (Fig. 4c). As can be seen, very good agreement is equally obtained for the dispersion slope over most of the 400 nm wide interval.

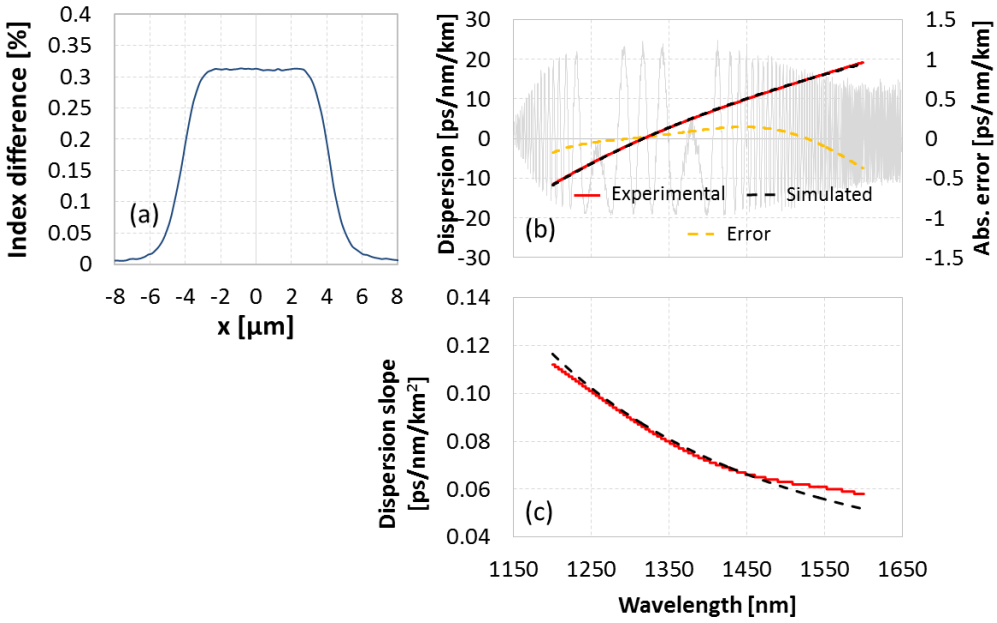

Fig. 4: Evaluation of the accuracy of the technique on a standard single mode fibre (SMF). (a) Measured refractive index profile of the SMF; (b) measured and simulated dispersion, (c) measured and simulated dispersion slope.

We implemented a fully automated setup using a PC and the Labview® development environment. The PC controls the two beam shutters S1 and S2 and the OSA so that the three spectra necessary for data analysis (interference spectrum, reference arm spectrum and fiber arm spectrum), are sequentially acquired. The dataset is then analysed with the algorithms based on the data analysis approach described in section 2. The dispersion profiles are promptly displayed on-screen without the need for any manual intervention during any part of the process. We typically obtain single-shot dispersion profiles in less than 10 s.

4. Dispersion measurement of key MOF fiber types

In order to further investigate the potential of our technique, we measured three microstructured fibers with very different dispersion properties: i) a lead silicate microstructured fiber exhibiting a flat and near-zero dispersion profile, ii) a hollow core photonic bandgap fiber characterized by high and strongly varying dispersion within its transmission window and finally, iii) a highly birefringent microstructured fiber exhibiting relatively low dispersion (<100 ps/nm/km) over a very broad range of wavelengths (~1000 nm). Besides having convenient dispersion profiles, these fibers have interesting applications, some of which have been demonstrated already in several of our ongoing research programs.

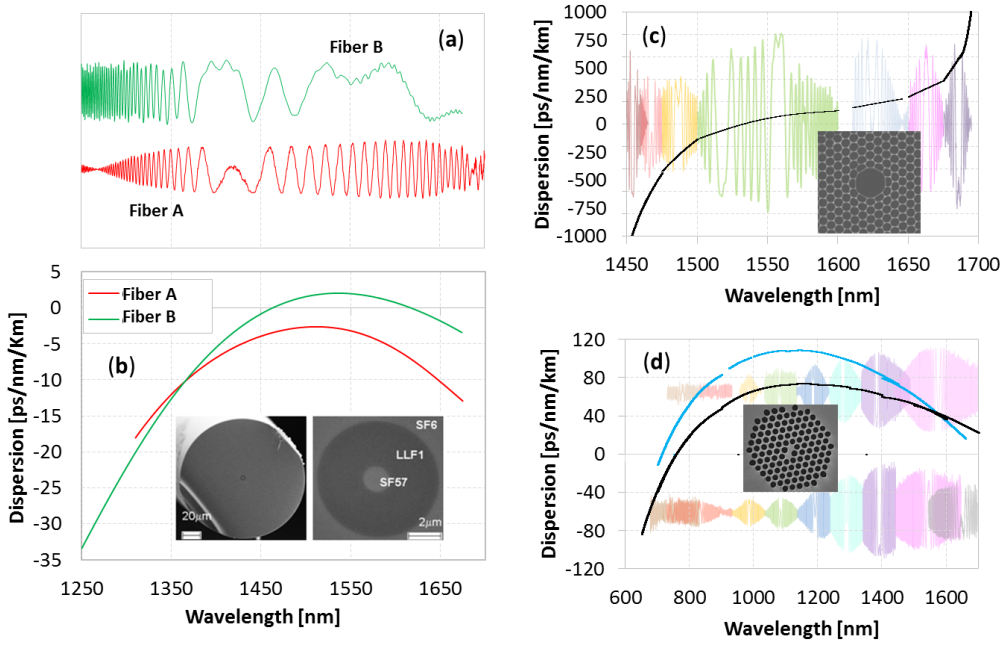

Fig. 5: Dispersion measurement results for three different types of microstructured optical fibers: (a) Highly nonlinear lead silicate fiber with W-type index profile: (top) interferograms measured for two fibers with slightly different core diameters (1.62 and 1.67 μm); (bottom) corresponding calculated dispersion curves (b) Hollow-core bandgap fiber with a 7 cell core structure; (c) highly birefringent index-guiding microstructured fiber: polarization resolved measurements.

The first example is an all-solid soft-glass microstructured fiber based on a combination of three different lead-silicate glasses arranged to produce a W-type index profile (as discussed in more detail in [2]). Such 'W-fiber' was designed to have high nonlinearity and a flat and near-zero dispersion profile at 1550 nm, as required in several nonlinear signal

processing applications [13, 14]. To accurately match the design target (maximum dispersion below a few ps/nm/km in the C-band), W-fibers with a few percent difference in their core diameters were fabricated by suitably changing the fiber drawing parameters. To resolve the small differences in dispersion, high measurement accuracy in the range ~1ps/nm/km were required. Fig. 5(a) shows the interferograms (top) and the corresponding dispersion profiles (bottom) obtained for two W-fibers having a ~4% difference in core diameter. As expected, these fibers show flat and near-zero dispersion profiles with differences in the maximum GVD values down to a few ps/nm/km. We conclude that our measurement method can resolve very small differences in the dispersion profiles as required. The knowledge of GVD profiles was useful to support further application work: the fiber having an all-normal dispersion profile (red trace) was successfully used for broadband wavelength conversion [2], while the one with two close ZDWs and a small amount of anomalous dispersion in between (<2.5 ps/nm/km, green trace) was used to demonstrate generation of a broad and flat supercontinuum at relatively low pump powers [15].

We then tested a hollow core photonic bandgap fiber (HC-PBGF) with a 7-cell core geometry, also designed for operation around 1550 nm. A scanning electron microscope (SEM) image is shown in the inset of Fig. 5(b). HC-PBGFs are resonant structures which guide light within a well-defined interval of wavelengths and typically have GVD profiles diverging both at the short and long wavelength bandgap edges [16]. This unusual dispersion profile enables us to further demonstrate the performance of our technique at high values of both dispersion and dispersion slope and to estimate the highest/lowest measurable dispersion. When the fiber dispersion is high, the interferograms have closely spaced spectral fringes and become narrower in width. Even using the highest feasible resolution compatible with temporal stability (high OSA resolutions require longer spectral acquisition times), we found that six to seven interferograms (obtained by suitably varying the length of the reference arm) were typically required to map the dispersion over the whole bandgap of the HC-PBGF, about ~250 nm in width. The full dispersion profile could then be obtained as a collection of neighboring curves, as shown in Fig. 5(b). The highest measurable dispersion, in this case about ±1000 ps/nm/km, is determined by the resolution of the OSA. It should be noted that 7 cell PBGFs are slightly multimode [17] and indeed several secondary interferograms, produced by higher order core modes, were observed to overlap with the primary interferogram of the fundamental (LP_{01}-like) mode. Whilst their intensity could be minimized by optimizing the input coupling, they could not be completely eliminated and their presence produced a slightly higher level of noise as compared, e.g. to what was observed in the case of SMF. Despite this, the curves obtained from adjacent interferograms were remarkably consistent (within ~5%); note that no interpolation or other data reduction treatment is applied to the dispersion data plotted in Fig. 5(b).

Last, we measured a highly birefringent, high nonlinearity index-guiding MOF incorporating a strongly asymmetric core (SEM in Fig.5(c)-inset). By adjusting the input half-wave plate, we obtained polarization resolved measurements along the two fiber axes. As this fiber has moderate GVD values (<100 ps/nm/km), it was possible to obtain data over a ~1000 nm wide interval (700-1700nm) by analyzing a set of 8 contiguous interferograms per each polarization. The corresponding GVD curves plotted in Fig. 5(c) are again remarkably consistent. Note that the measurement range is limited by the bandwidth of the components and the OSA range only.

7. Conclusion

We have reported a dispersion measurement based on a direct phase extraction method that provides for fast, high accuracy and ~ps/nm/km absolute precision measurements over broad spectral intervals several hundred nm wide using single shot interferograms. The method, based on a state-of-the-art supercontinuum source, is relatively simple to implement, uses widely available optical components and is amenable to being extensively automatized. To

achieve high measurement precision and accuracy we investigated systematically sources of environmental noise and we have eliminated the systematic error introduced by optical components used within the set-up used. The accuracy and absolute precision estimated from measurements on a standard single mode fibre over a 400nm wide interval (1200-1600nm) were <0.5 ps/nm/km and <0.1 ps/nm/km, respectively, for spectra collected in as little as 10s. To fully illustrate its potential and the versatility, we have successfully applied our method to measure microstructured fibers having markedly different dispersion profiles. The technique is ideally suited to resolve differences arising due to very small structural variations and can cope with dispersion profiles having extreme curvature or dispersion values as high as 1000 ps/nm/km. For fibers with more moderate values of dispersion (~100 ps/nm/km), measurements over intervals exceeding 1000 nm are possible by collecting multiple adjacent interferograms.

Acknowledgments

This work was supported by the UK EPSRC through grant EP/H02607X/1 and EP/I01196X/1.